

Spiroepoxytriazoles Are Fumagillin-like Irreversible Inhibitors of MetAP2 with Potent Cellular Activity

Michael Morgen,^{†,⊥} Christian Jöst,^{‡,⊥} Mona Malz,[†] Robert Janowski,[§] Dierk Niessing,^{§,||} Christian D. Klein,[‡] Nikolas Gunkel,[†] and Aubry K. Miller^{*,†}

[†]Cancer Drug Development Group, German Cancer Research Center (DKFZ), Im Neuenheimer Feld 280, D-69120 Heidelberg, Germany

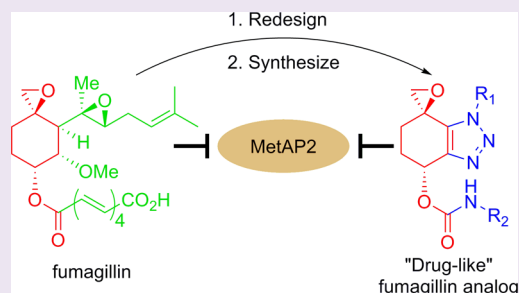
[‡]Medicinal Chemistry, Institute of Pharmacy and Molecular Biotechnology (IPMB), Heidelberg University, Im Neuenheimer Feld 364, D-69120 Heidelberg, Germany

[§]Institute of Structural Biology, Helmholtz Zentrum München, German Research Center for Environmental Health (HMGU), D-85764 Neuherberg, Germany

^{||}Biomedical Center of the Ludwig-Maximilians-Universität München, D-82152 Planegg-Martinsried, Germany

S Supporting Information

ABSTRACT: Methionine aminopeptidases (MetAPs) are responsible for the cotranslational cleavage of initiator methionines from nascent proteins. The MetAP2 subtype is up-regulated in many cancers, and selective inhibition of MetAP2 suppresses both vascularization and growth of tumors in animal models. The natural product fumagillin is a selective and potent irreversible inhibitor of MetAP2, and semisynthetic derivatives of fumagillin have shown promise in clinical studies for the treatment of cancer, and, more recently, for obesity. Further development of fumagillin derivatives has been complicated, however, by their generally poor pharmacokinetics. In an attempt to overcome these limitations, we developed an easily diversifiable synthesis of a novel class of MetAP2 inhibitors that were designed to mimic fumagillin's molecular scaffold but have improved pharmacological profiles. These substances were found to be potent and selective inhibitors of MetAP2, as demonstrated in biochemical enzymatic assays against three MetAP isoforms. Inhibitors with the same relative and absolute stereoconfiguration as fumagillin displayed significantly higher activity than their diastereomeric and enantiomeric isomers. X-ray crystallographic analysis revealed that the inhibitors covalently modify His231 in the MetAP2 active site via ring-opening of a spiroepoxide. Biochemically active substances inhibited the growth of endothelial cells and a MetAP2-sensitive cancer cell line, while closely related inactive isomers had little effect on the proliferation of either cell type. These effects correlated with altered N-terminal processing of the protein 14-3-3-γ. Finally, selected substances were found to have improved stabilities in mouse plasma and microsomes relative to the clinically investigated fumagillin derivative beloranib.



Natural products have been an excellent source of leads for drug development, particularly in the areas of antibiotic and anticancer therapies where natural products (and their derivatives) comprise a significant percentage of clinically used drugs.¹ Sometimes a natural product can be developed into a drug, but often structural modifications to a natural product's scaffold are required to improve its pharmacological properties such that it can successfully be administered to human patients. Due to the structural complexity of many natural products, semisynthetic approaches are often the method of choice for optimization campaigns. A limitation to this approach is that the resulting diversification strategies may be largely opportunistic in nature, guided by issues of synthetic convenience and practicality, i.e., where the molecule can selectively be modified. A natural product where such an approach has been applied is fumagillin (**1**), a metabolite of the fungus *Aspergillus fumigatus* (Figure 1).^{2–13}

Interest in the biological properties of **1** initially stemmed from Ingber and Folkman's serendipitous discovery that it selectively inhibits the growth of endothelial cells at subnanomolar concentrations,² propelling studies first into its use as an antiangiogenic cancer therapy¹⁴ and, more recently, in obesity indications, where beloranib (**3**) is currently investigated in a number of phase 2 and 3 trials.¹⁵ Studies to identify fumagillin's primary biological target^{16–18} eventually resulted in an X-ray crystal structure of **1** bound to methionine aminopeptidase 2 (MetAP2),¹⁹ a metalloprotease responsible for the cotranslational cleavage of initiator methionines from ribosomally synthesized proteins. Subsequent studies identified the cell cycle regulator p21 as the furthest downstream effector of fumagillin's inhibitory activity on endothelial cells,^{20,21} but

Received: September 21, 2015

Accepted: December 18, 2015

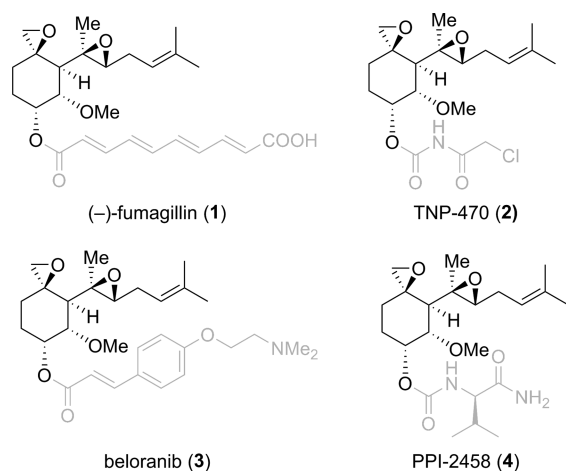


Figure 1. Fumagillin and clinically investigated derivatives. The conserved fumagillol core is depicted in black, while side chain variations are depicted in gray.

the mechanistic steps that link MetAP2 inhibition to p21 activation are still incompletely understood.^{22,23} Similarly, the connection between fumagillin-based MetAP2 inhibition and weight loss is still under investigation, and nonenzymatic suppression of ERK1/2 phosphorylation has been implicated.^{15,24}

MetAP2 is irreversibly inhibited by fumagillin via covalent bond formation between the spiro-oxirane C2 and a histidine residue (His231) in the active site of the enzyme (Figure 2).

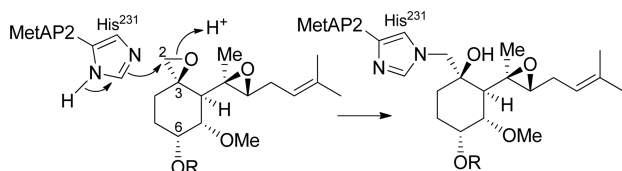


Figure 2. Covalent inhibition of MetAP2 by fumagillin.

While the isoprenoid side-chain of **1** is critical for MetAP2 binding by filling a hydrophobic pocket of the enzyme and simultaneously positioning the oxirane moiety for reaction, the polyunsaturated C6 side chain is solvent-exposed and not required for activity.

The lack of a strict structural requirement at C6, coupled with the ease by which the C6 ester moiety can be hydrolyzed (to fumagillol) and the resulting secondary hydroxyl group further modified, enabled a range of structure–activity relationship (SAR) studies at this position.^{2–4,7,8,13} Indeed, modifications to the fumagillin structure were required because clinical studies with **1** and its derivative TNP-470 (**2**, Figure 1) were hampered by the poor pharmacological properties of the two substances, in particular extremely short plasma half-life (~2 min)²⁵ and CNS-related side effects.²⁶ More recently developed derivatives like **3** and PPI-2458 (**4**) have improved pharmacological profiles (no CNS effects) but still suffer from relatively poor pharmacokinetics.^{27,28} For this reason, **3** is currently administered as a subcutaneous suspension.

While compounds like **3** and **4** demonstrate that modifications at C6 have the potential to alleviate some of the pharmacological weaknesses associated with fumagillin, such modifications will never be able to overcome liabilities inherent to the fumagillol substructure, e.g., metabolic

instability in the isoprenoid side-chain.^{28,29} We chose to address this problem through a *de novo* synthesis approach, which would allow us to explore chemical space that is inaccessible when using the natural product as a starting material and designed a new class of spiro-epoxide containing MetAP2 inhibitors that are structurally inspired by fumagillin.^{30–35} The principle of our design was that these compounds should (1) be stereochemically less complex than fumagillin, (2) incorporate synthetically accessible and potentially drug-like nitrogen-containing heterocycles, and (3) closely resemble fumagillin's three-dimensional structure so as to maintain its highly optimized intermolecular fit into the target enzyme. Taking into account previous SAR data, our own design principles, and using molecular models, we hypothesized that tetrahydrobenzotriazoles of the general structures **5** would be fumagillin-like inhibitors, while cognizant of the risks associated with such a scaffold jump (Figure 3). We report, herein, the

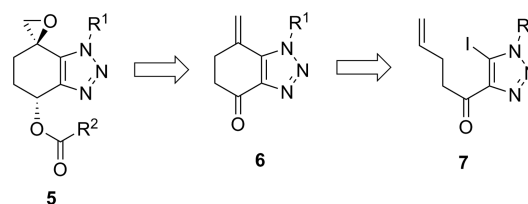


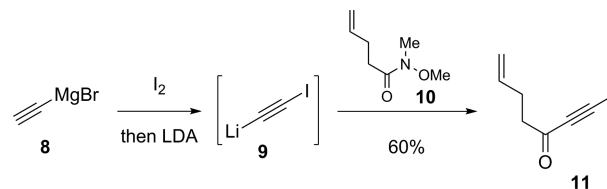
Figure 3. Retrosynthetic analysis of target compound **5**.

synthesis of such a chemical series, and the characterization of certain members as potent and selective MetAP2 inhibitors which covalently modify His231 in the active site of the enzyme. Moreover, active substances exhibit on-target growth inhibition of endothelial cells, reduced proliferation of a MetAP2-sensitive cancer cell line, and improved plasma and microsomal stabilities relative to beloranib.³⁶

RESULTS AND DISCUSSION

Synthesis of Epoxytriazoles. At the outset of this project, there were no published approaches to spiroepoxy tetrahydrobenzotriazoles **5** or their envisioned precursors **6**. Moreover, we were concerned that the intermediates **6**, upon formation, would spontaneously aromatize to the corresponding hydroxybenzotriazoles. Nevertheless, motivated by the potential to rapidly synthesize a library of fumagillin analogs, we planned to access compounds like **6** via Heck cyclization of iodoalkenes like **7**. In the forward sense, our synthetic route began with a one-pot reaction (Scheme 1): Iodination and subsequent deprotonation of ethynylmagnesium bromide (**8**) gave lithium iodoacetylide (**9**) which reacted with Weinreb amide **10**³⁷ to give iodoynone **11**, a compound prone to decomposition and

Scheme 1. Synthesis of Iodoynone **11**^a

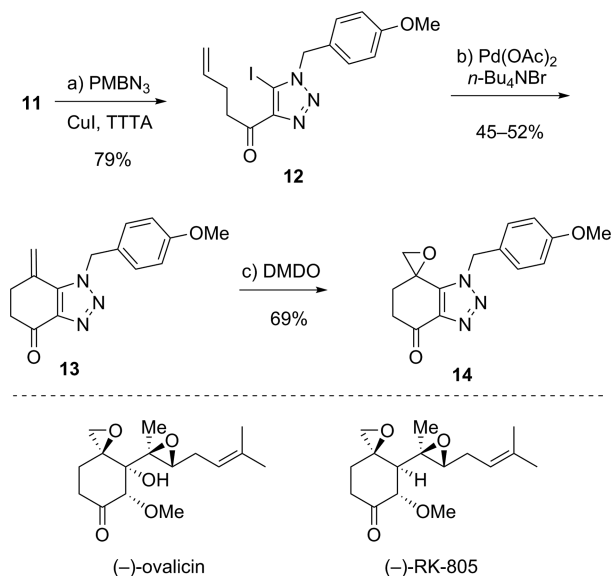


^aReagents and conditions: I₂ (1.0 equiv), THF, −78 to 0 °C, 1 h, then LDA (1.0 equiv), −78 to 0 °C, 30 min, then **10** (1.0 equiv), −78 °C to −20 °C, 2 h, 60%.

that we were unable to prepare from the corresponding terminal ynone, but which could be reliably prepared on a 50 mmol scale in this manner.^{38,39}

Alkyne **11** could be coupled with a variety of azides in copper catalyzed Huisgen cyclizations to generate iodotriazoles of the general structure **7**.⁴⁰ For example, reaction with 4-methoxybenzyl azide (PMBN₃) cleanly gave trisubstituted triazole **12** as a single regioisomer (Scheme 2). Most attempts to form bicycle

Scheme 2. Representative Ketoepoxide Synthesis^a



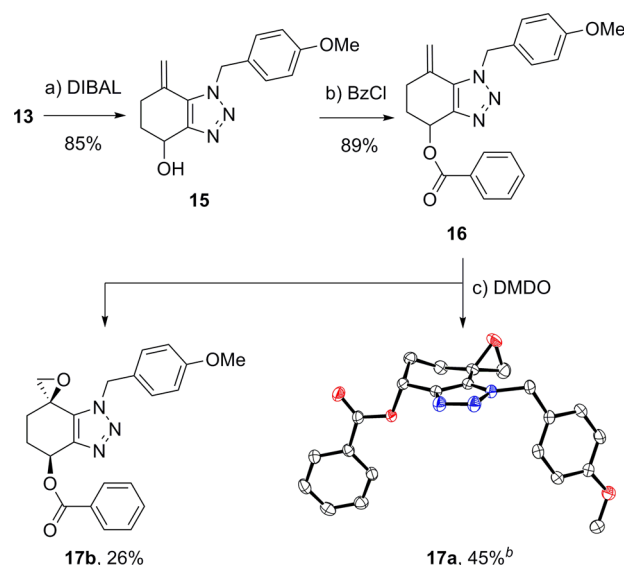
^aReagents and conditions: (a) PMBN₃ (1.0 equiv), CuI (5 mol %), TTTA (5 mol %), THF, RT, 79%; (b) Pd(OAc)₂ (10 mol %), *n*-Bu₄NBr (1.0 equiv), Na₂CO₃ (2.5 equiv), MeCN/H₂O (9:1), 70 °C, 24 h, 52%; (c) DMDO (0.09 M in acetone, 2.0 equiv), CH₂Cl₂, RT, 18 h, 69%.

13 from **12** via Heck cyclization resulted either in no reaction or complete consumption of the starting material with very low yields of the desired product.⁴¹ After extensive experimentation, we found that Jeffery's phase transfer method under rigorously degassed conditions gave a reliable 45–52% yield of **13** (the isomeric aromatized hydroxybenzotriazole was isolated in 15% yield).⁴² Epoxidation of **13** with DMDO cleanly provided racemic epoxide **14**, an analog of the naturally occurring fumagillin congeners ovalicin and RK-805.

Alternatively, DIBAL reduction of ketone **13** gave alcohol **15** (Scheme 3). This alcohol could be acylated to, for example, **16** and subsequently oxidized with DMDO to give the separable racemic epoxides **17a/17b** in equal amounts (determined by ¹H NMR of the crude reaction mixture), indicating essentially no diastereoselectivity for the epoxidation reaction. The relative stereochemistry of the two compounds was confirmed via crystallographic analysis of single crystals grown from **17a**, which revealed this diastereomer to have the fumagillin-like “anti” relationship of the oxirane and carboxylate oxygens at C3 and C6, respectively (fumagillin numbering).

Biochemical MetAP2 Inhibition. We prepared a series of alkyl and substituted benzyl triazoles in analogy to ketoepoxide **14** and measured their inhibitory activity against *E. coli* MetAP (*Ec*MetAP), human type 1 MetAP (*Hs*MetAP1), and human type 2 MetAP (*Hs*MetAP2) at 25 μM inhibitor concentration.⁴³ Using the tetrapeptide substrate MGMM, inhibition was

Scheme 3. Representative Synthesis of Diastomeric C6 O-acyl Epoxides^a

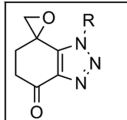


^aReagents and conditions: (a) DIBAL (1.6 equiv), CH₂Cl₂, −78 °C, 30 min, 85%; (b) benzoyl chloride (1.2 equiv), Et₃N (1.4 equiv), DMAP (10 mol %), CH₂Cl₂, RT, 18 h, 89%; (c) DMDO (0.09 M in acetone, 2.0 equiv), CH₂Cl₂, 45 min, 45% of **17a** and 26% of **17b**. ^bThermal ellipsoid representation (50% probability) of **17a**: C (white); O (red); N (blue).

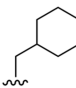
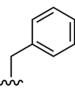
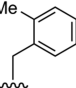
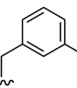
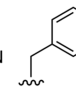
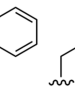
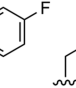
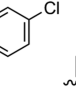
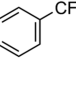
measured via HPLC quantification of the product GMM. All compounds were found to be essentially inactive against both *Ec*MetAP and *Hs*MetAP1 while some were effective inhibitors of *Hs*MetAP2. Dose–response IC₅₀ values against *Hs*MetAP2, after a 20 min preincubation of inhibitor and enzyme, were then determined for compounds with reasonable potency (Table 1). While the alkyl side-chain derivatives (**18–21**) were poorly active against *Hs*MetAP2, the benzyl derivatives showed much more promising activity, with many (**14**, **25–28**) giving submicromolar IC₅₀ values. Both *ortho* (**23**) and *meta* (**24**) substitutions were tolerated, as well as a larger 2-naphthyl substitution (**25**), but *para* substitutions (**14**, **26–28**) appeared the most promising. Epoxide precursors **13** and **16** were found to be inactive against *Hs*MetAP2, indicating that the epoxide moiety is required for activity and suggesting that the compounds are covalent inhibitors.

We then tested a series of compounds in the **17a/17b** series and found that many of these substances were also selective *Hs*MetAP2 inhibitors (Table 2, Supporting Information Table 3). Interestingly, compounds with a fumagillin-like “anti” relationship between heteroatoms at C3 and C6 (**17a**, **29a**, **30a**, **31a**) were significantly more active than their “syn” counterparts (**17b**, **29b**, **30b**, **31b**, respectively). The latter were quite poor inhibitors, giving circumstantial evidence that the binding mode is similar to fumagillin. Compounds with a hydrolytically more stable carbamate, instead of ester, linkage (**30a**, **31a**, **32–35**) were generally highly active compounds with **31a** having an IC₅₀ value of 220 nM. Compound **35** was also a submicromolar inhibitor, indicating that the carbamate linkage could be modulated. The most active substance, **31a**, was separated into its component enantiomers, (+)-**31a** and (−)-**31a**, via chiral chromatography, and (+)-**31a** was found to be entirely responsible for the biochemical activity of the

Table 1. Biochemical Activities of Ketoepoxide Inhibitors^a



R = Me Et *n*Pr

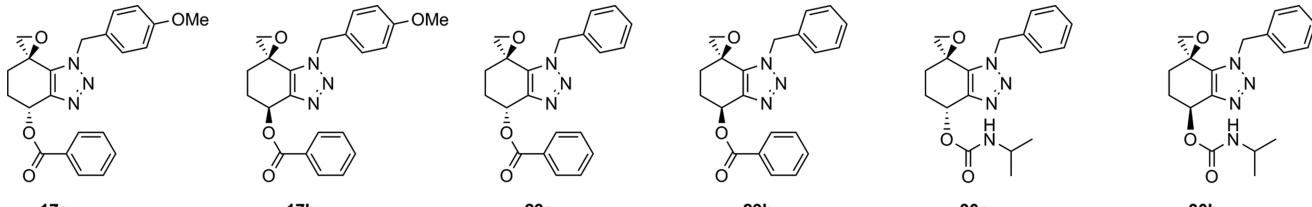
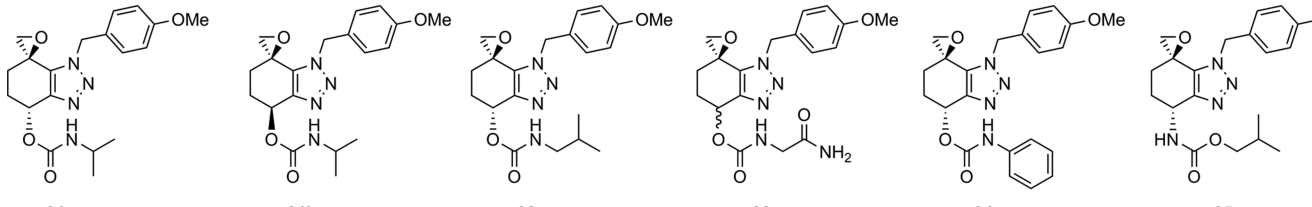










18 19 20 21 22 23 24 25 26 27 28 14

Cmpd.	<i>EcMetAP</i> ^b	<i>HsMetAP</i> 1 ^b	<i>HsMetAP</i> 2 ^b	<i>HsMetAP</i> 2 IC ₅₀ (μM)	Cmpd.	<i>EcMetAP</i> ^b	<i>HsMetAP</i> 1 ^b	<i>HsMetAP</i> 2 ^b	<i>HsMetAP</i> 2 IC ₅₀ (μM)
18	20 ± 2	n.i.	n.i.	—	25	24 ± 8	n.i.	100	0.59 ± 0.07
19	22 ± 5	n.i.	n.i.	—	26	n.i.	n.i.	100	0.25 ± 0.05
20	21 ± 5	n.i.	25 ± 2	—	27	n.i.	n.i.	100	0.52 ± 0.13
21	19 ± 5	n.i.	40 ± 3	>50	28	n.i.	n.i.	100	0.44 ± 0.01
22	n.i.	n.i.	64 ± 1	2.9 ± 0.4	14	n.i.	n.i.	100	0.46 ± 0.09
23	n.i.	n.i.	100	2.3 ± 0.7	13	24 ± 5	n.i.	n.i.	—
24	n.i.	n.i.	100	1.1 ± 0.2	16	n.i.	n.i.	32 ± 1	>50

^aEach data set was measured in triplicate (mean ± standard deviation); n.i. = not inhibited (<15% inhibition value). ^bValues are reported as percent inhibition at 25 μM inhibitor concentration with respect to a solvent control.

Table 2. Biochemical Activities of C6-Stereogenic Epoxide Inhibitors^a

											
17a		17b		29a		29b		30a		30b	
											
31a		31b		32		33		34		35	
Cmpd.	HsMetAP2 IC ₅₀ (μM)			Cmpd.	HsMetAP2 IC ₅₀ (μM)			Cmpd.	HsMetAP2 IC ₅₀ (μM)		
17a	0.93 ± 0.08			30b	46 ± 7			34	0.99 ± 0.05		
17b	35 ± 6			31a	0.22 ± 0.03			35	0.6 ± 0.1		
29a	1.4 ± 0.3			31b	>50			(+)-31a	0.22 ± 0.03		
29b	>50			32	0.60 ± 0.22			(-)-31a	>50		
30a	0.78 ± 0.26			33 ^b	1.21 ± 0.30			(+)-31b	43 ± 5		
								(-)-31b	>50		

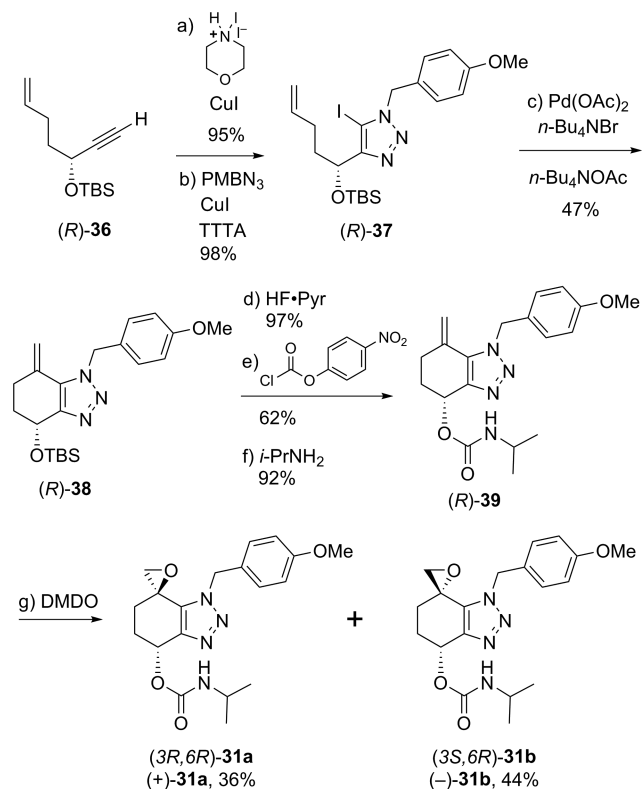
^aEach data set was measured in triplicate (mean ± standard deviation). ^b33 was an unseparable 1:1 mixture of diastereomers.

racemate. As expected, the component enantiomers of 31b, (+)-31b, and (−)-31b were found to be inactive.

Asymmetric Synthesis of (+)-31a. In order to determine the absolute configuration of (+)-31a, an enantioselective synthesis was developed as shown in Scheme 4. Starting with known protected alcohol (R)-36 (>95% ee),³⁷ iodination followed by copper catalyzed Huisgen cyclization gave triazole (R)-37. Heck cyclization under Jeffery conditions with (R)-37 was much slower than with 12 and its congeners, and while it could be driven to completion over 96 h with repeated catalyst loadings, yields were always well below 50%. Ultimately, “solventless” conditions were found to be superior, the reaction completing in a few hours with lower catalyst loading to give (R)-38 in a yield of 47%.⁴⁴ Silyl deprotection of (R)-38 gave alcohol (R)-15, which could be converted in two steps to carbamate (R)-39 and, ultimately, to the epoxides (3R,6R)-31a and (3S,6R)-31b. The first product was found to have a positive

optical rotation ([α]_D²² +46.5°). Moreover, this substance was found to have an IC₅₀ value against MetAP2 and a chiral HPLC retention time identical to the chromatographically separated active enantiomer (+)-31a. This indicates that the active enantiomer and fumagillin share the same absolute configuration at C3 and C6. The optical rotation of (3S,6R)-31b was negative ([α]_D²² −12.5°), thereby defining the absolute stereochemistry of all four stereoisomers (Figure 4).

Crystal Structure Confirms Covalent Inhibition. As stated above, the requirement of the epoxide moiety for inhibitory activity is suggestive that the compounds are, like fumagillin, covalent inhibitors. Time dependent inhibition studies with 31a, 32, and 33 supported this hypothesis (Supporting Information Figure 3). Moreover, the fact that structurally similar substances exhibited very different biochemical activities (e.g., (±)-31a vs (±)-31b and (+)-31a vs (−)-31a) suggested that the substances are quiescent affinity

Scheme 4. Asymmetric Synthesis of (+)-31a^a

^aReagents and conditions: (a) NIM (1.2 equiv), CuI (5 mol %), THF, RT, 18 h, 95%; (b) PMBN₃ (1.1 equiv), CuI (5 mol %), TTTA (5 mol %), THF, RT, 98%; (c) Pd(OAc)₂ (10 mol %), *n*-Bu₄NBr (10.0 equiv) *n*-Bu₄NOAc (5.0 equiv), 100 °C, 2 h, 47%; (d) HF·Pyr, pyridine, THF, RT, 3 h, 97%; (e) *p*-nitrophenyl chloroformate (2.0 equiv), Et₃N (2.0 equiv), DMAP (0.3 equiv), CH₂Cl₂, RT, 1.5 h, 62%; (f) *i*-PrNH₂ (5.5 equiv), *i*-Pr₂NEt (2.9 equiv), EtOH, RT, 20 h, 92%; (g) DMDO (0.09 M in acetone, 1.6 equiv), CH₂Cl₂, 36% of (+)-31a and 44% of (−)-31b.

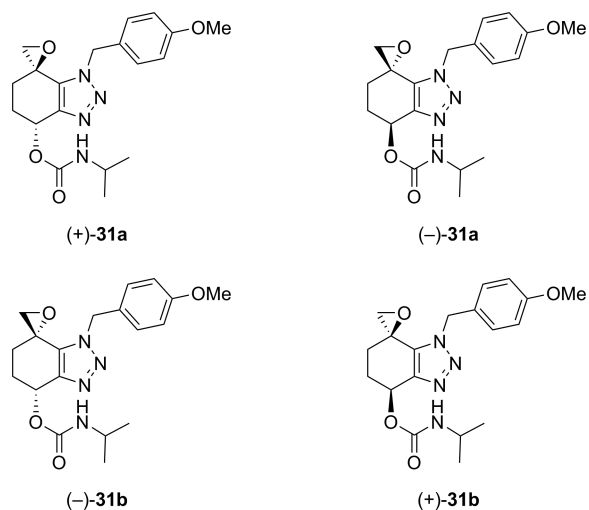


Figure 4. Depiction of the four stereoisomers of compound 31.

labels with some reversible binding to the active site and only make a covalent bond in a proximity-promoted second step.⁴⁵ This supposition was supported by solution of the X-ray crystal structure of one molecule of (+)-31a bound to HsMetAP2 at a resolution of 1.75 Å (Figure 5, panel A; PDB code 5CLS). In

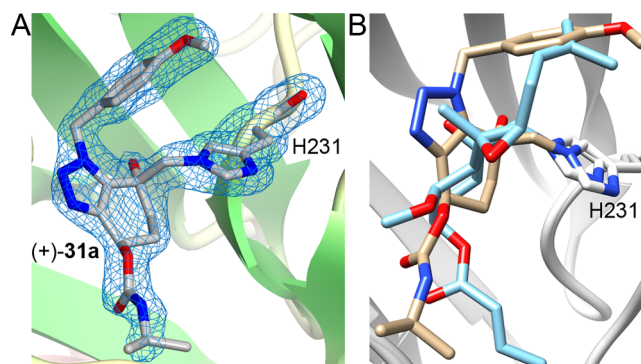


Figure 5. (A) X-ray crystal structure of (+)-31a at 1.75 Å resolution (*R* = 16.0%, *R*_{free} = 18.9%) covalently bound to HsMetAP2 at His231 (PDB code 5CLS). (B) Overlay of (+)-31a (tan carbon framework) and fumagillin (PDB code 1BOA, light blue carbon framework) bound to MetAP2.

analogy to fumagillin, and as per our design plan, His231, in the active site of the enzyme, was found to be covalently linked to (+)-31a at the (formerly) epoxide C2 carbon. The 4-methoxybenzyl group of (+)-31a fills the same hydrophobic pocket as fumagillin's prenyl side chain, and the carbamate side chain is solvent exposed, like fumagillin's polyene side chain. Soaking MetAP2 crystals with (−)-31a at a concentration of 50 mM never produced any detectable electron density associated with a bound inhibitor.

While the protein-inhibitor structures of (+)-31a and fumagillin bound to MetAP2 show some similarities, an overlay of the two structural models also reveals differences (Figure 5, panel B). The imaginary planes defined by the central six-membered rings of the two inhibitors intersect each other at an angle of ~30°. In addition, while fumagillin's cyclohexane ring adopts a chair configuration with the epoxide-derived hydroxyl group oriented axially, the six-membered ring of (+)-31a adopts a half-chair conformation with the analogous hydroxyl group oriented in a pseudoequatorial position. Interestingly, while both fumagillin and (+)-31a fill the same hydrophobic pocket, their side chains take different "trajectories" to reach the back of the pocket. This indicates that there may be room to "grow" our inhibitors so as to improve their potencies further.

In contrast to (−)-31a, individually soaking MetAP2 crystals with (−)-31b and (+)-31b gave well-defined X-ray structures showing electron density for each compound. The substance (−)-31b (Figure 6, panel A; PDB code 5D6E) has a pose similar to (+)-31a in the enzymatic pocket (Figure 6, panel B) but was found to be covalently bound via Glu364, an amino acid that normally chelates one of the two cobalt atoms in the active site. This can be understood because (−)-31b is epimeric to (+)-31a at C3 and, upon binding to MetAP2, presents the oxirane oxygen, instead of the C2 methylene, toward His231. While this orientation precludes S_N2 ring-opening by His231, Glu364, on the opposite side of the enzymatic pocket, is able to do so. Compound (+)-31b, epimeric with (+)-31a at C6, was found covalently bound to His231 but adopts a half-chair conformation that is ring-flipped relative to (+)-31a (Figure 6, panel C; Figure 6, panel D, PDB code 5D6F). Presumably, in the case of (−)-31b and (+)-31b, the "forcing" conditions of the crystallization experiments (high inhibitor concentrations, covalent mechanism, long reaction times) drive the reaction of the inhibitors with MetAP2, even though their noncovalent affinity may be relatively low. Nevertheless, in spite of the low

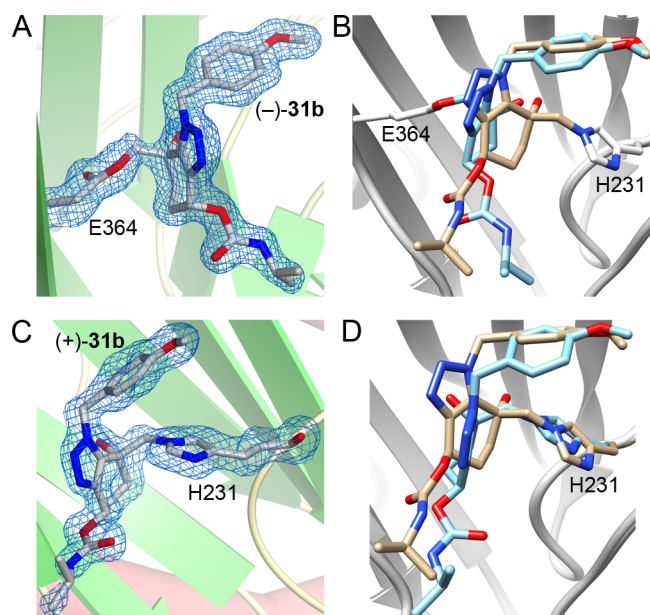


Figure 6. (A) X-ray crystal structure of (–)-31b at 1.49 Å resolution ($R = 11.0\%$, $R_{\text{free}} = 15.6\%$) covalently bound to HsMetAP2 at Glu364 (PDB code 5D6E); (B) X-ray crystal structure overlay of (+)-31a (tan) and (–)-31b (blue); (C) X-ray crystal structure of (+)-31b at 1.55 Å resolution ($R = 14.7\%$, $R_{\text{free}} = 18.5\%$) covalently bound to HsMetAP2 at His231 (PDB code 5D6F); (D) X-ray crystal structure overlay of (+)-31a (tan) and (+)-31b (blue).

biochemical activity of (+)-31b and (–)-31b, no nucleophilic solvent-exposed residues (e.g., Lys427 or Cys290) other than His231 were modified, further underlining the selective binding behavior of this compound class.

Cellular and Biochemical Data Correlate. The epoxides (±)-31a, (±)-31b, (+)-31a, and (–)-31a were tested for their ability to arrest the growth of human umbilical vein endothelial cells (HUVECs) and were found to have activities that correlated with their biochemical MetAP2 activities. Whereas (±)-31a inhibited the growth of HUVECs with an EC_{50} of 165 nM, (±)-31b was much less effective, with an EC_{50} of 6 μM (Figure 7, panel A). As expected, the active enantiomer (+)-31a potentially affected the growth of HUVECs with an EC_{50} of 94 nM, while (–)-31a showed no effect up to 10 μM . Similar observations were made when HT1080 cells, a cell line known to be sensitive to MetAP2 inhibition, were treated with these four compounds (Figure 7, panel B).⁴⁶ Consistent with fumagillin-based inhibitors, an incomplete reduction of cell number was observed in both cell lines. In HUVECs, it is well-known that, at low concentrations, fumagillin-based inhibitors have a cytostatic effect; i.e., cells no longer divide but remain viable. Only at much higher concentrations do the inhibitors become cytotoxic.⁴⁷ A similar result was found when beloranib was tested against HT1080 cells (Supporting Information Figure 4).

The adaptor protein 14-3-3- γ has been shown to be a useful cellular marker for MetAP2 activity.⁴⁸ Proteolytic removal of the N-terminal methionine from 14-3-3- γ was strongly altered by (+)-31a in HUVECs, whereas little effect was observed with (–)-31a (Figure 7C). Together with the biochemical and cellular data, these results are consistent with the observed cellular phenotype resulting from on-target MetAP2 inhibition.

Carbamates Are More Stable than Beloranib. The primary clinical drawback of fumagillin-based substances, like

beloranib, are poor pharmacokinetics, in particular low metabolic stability. In order to gain insight into the pharmacokinetic properties of our compounds, stability tests in mouse plasma were conducted in comparison to beloranib. While the tested ketone and ester containing substances (14, 28, 29a) had relatively poor stability profiles, the carbamates (30a, (±)-31a) had half-lives that were ~ 2.0 times longer than beloranib (Figure 8, panel A). In another experiment, beloranib and (+)-31a were tested in mouse liver microsomes. Beloranib was found to have a half-life of less than 5 min, while (+)-31a had a significantly longer half-life of 40 min (Figure 8, panel B).

Conclusion. The development of MetAP2 inhibitors has been, and continues to be, an area of intense research. While interest in MetAP2 inhibitors was initially focused on oncology, the potential for MetAP2 inhibitors as drugs targeting obesity has recently expanded their therapeutic potential. MetAP2 inhibitors which are based on the fumagillin substructure have been studied extensively, and their irreversible mode of action distinguishes them from reversible inhibitor scaffolds, which generally rely on metal chelating functional groups for potency.¹⁴

While nature has evolved fumagillin to be a near perfect inhibitor in terms of potency and selectivity, attempts to use fumagillin as a drug in clinical trials have failed due to suboptimal ADME properties and poor pharmacokinetics. Campaigns to optimize these properties through modulation of the fumagillin C6 side chain have produced substances with improved profiles (e.g., 3 and 4), but these compounds retain liabilities inherent to the fumagillol scaffold.

Here, we introduce a new MetAP2 inhibitor scaffold that, while inspired by the structure of fumagillin, lacks the fumagillol core and, therefore, may have the potential for superior pharmacological properties. Our successful route to the compounds enabled the synthesis of a small but diverse set of compounds. Initial SAR analysis revealed that benzyl substitution on the triazole ring was optimal for effective MetAP2 inhibition and low activity against two other MetAP subtypes. Substances that are stereogenic at both C3 and C6 must display an “anti” relationship between the C3 oxygen and the C6 side chain; the “syn” diastereomers are completely inactive. Moreover, only one enantiomer of such an “anti”-configured compound is responsible for the activity of the inhibitors, and the absolute configuration of this enantiomer matches that of the natural product fumagillin.

The X-ray crystal structure of (+)-31a bound to MetAP2 reveals a covalent bond to His231, a mode of action identical to fumagillin. The binding pose is also similar to fumagillin, but differences between the two structures indicate that there may be additional space in the hydrophobic pocket to design further derivatives with enhanced binding. An expanded SAR study of allowed substitution patterns on the benzyl side chain could help uncover more potent substances.

The differential biochemical activities of the stereoisomers of compounds 31a and 31b were replicated in a cellular context. In both HUVECs and HT1080 cells, the “anti”-configured substance 31a was more potent than 31b. Similarly, the enantiomer (+)-31a was far more active in both cell lines than (–)-31a. An increase in the unprocessed form of 14-3-3- γ was observed in a dose-dependent manner for (+)-31a in HUVECs, while no change was observed with (–)-31a. Finally, carbamate substituted analogs 30a and 31a showed longer half-lives, relative to beloranib, in plasma and microsomal stability assays.

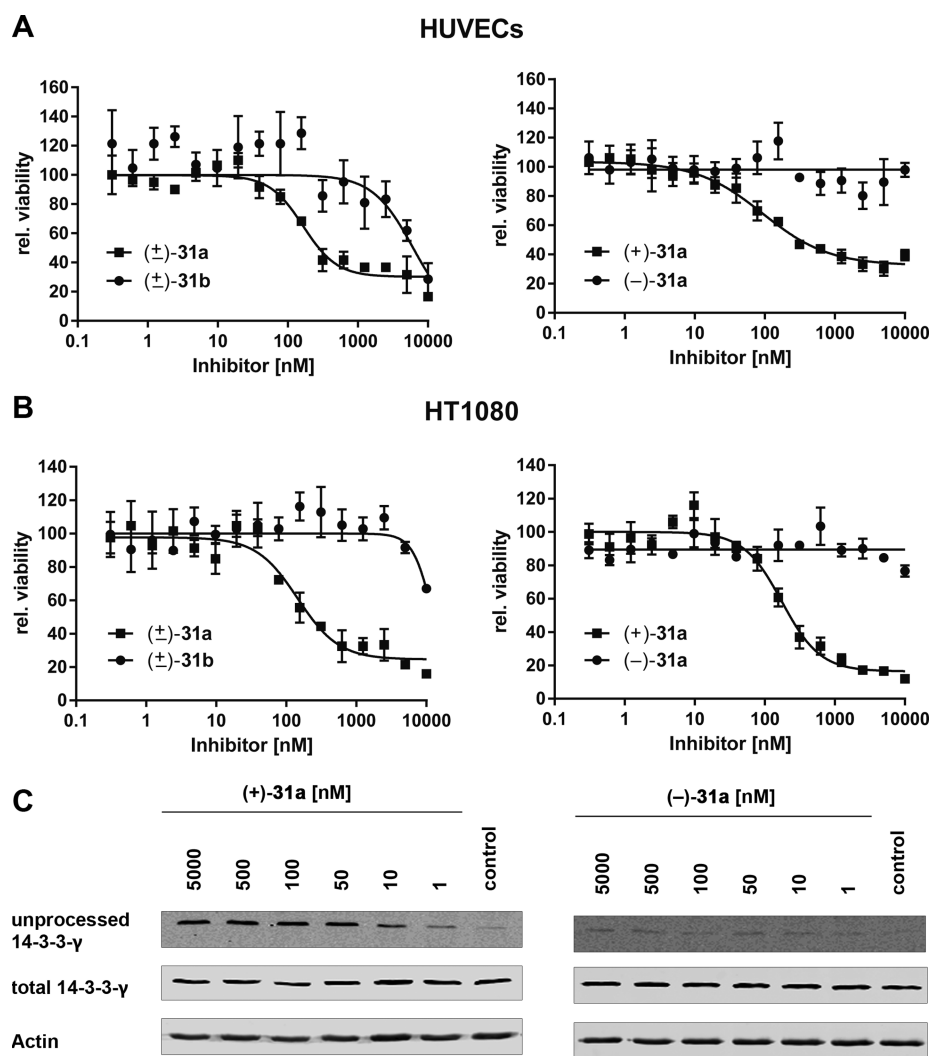


Figure 7. Dose–response curves for HUVECs (A) or HT1080 cells (B) when treated with inhibitor. Values represent triplicate means \pm SD. (C) Western blots for unprocessed 14-3-3- γ (only proteins with an N-terminal methionine are stained) versus total 14-3-3- γ levels when treated with inhibitor at the indicated concentrations or DMSO control.

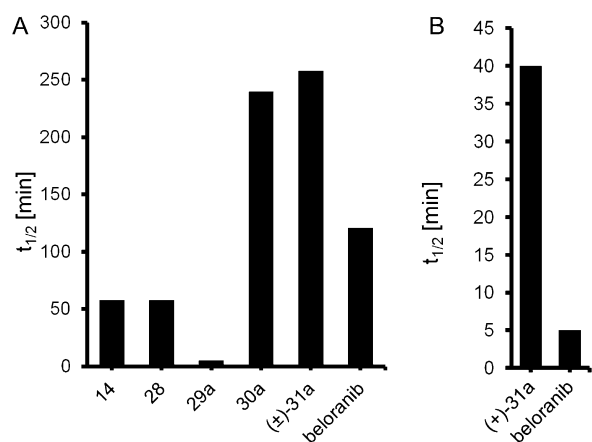


Figure 8. (A) Compound stability in mouse plasma. (B) Compound stability in mouse microsomes. (A and B) Each data set represents the mean of two independent measurements made with both positive and negative control substances.

While these data indicate that the compounds exert their cellular phenotype via irreversible MetAP2 inhibition and have

the potential for good pharmacokinetic properties, their cellular activity remains lower than fumagillin-based derivatives, which have picomolar IC_{50} growth-inhibition values against HUVECs. The further development of this class of compounds would, therefore, be enabled by the discovery of analogs that close the gap with fumagillin-based substances in terms of cellular potency. Additionally, a more thorough analysis of ADME properties and, ultimately, pharmacokinetics in animal models will be necessary to evaluate their real clinical potential.

In summary, we have reported the synthesis and preliminary biological evaluation of a new chemical class of spiroepoxide tetrahydrobenzotriazoles, inspired by the natural product fumagillin. These compounds are potent and selective inhibitors of MetAP2, as demonstrated in biochemical enzymatic assays. Their mode of action (covalent modification of the active site His231 residue) was confirmed to be identical to fumagillin via X-ray crystallography, and they are effective HUVEC growth inhibitors. With metabolic stabilities as good as or superior to the clinical candidate belorinib, this novel class of inhibitors potentially provides an alternative to fumagillin-based inhibitors.

METHODS

Synthetic Chemistry. Reaction mixtures were magnetically stirred in oven-dried glassware under a blanket of argon. External bath temperatures were used to record all reaction mixture temperatures. Reagents were purchased at the highest level of commercial quality and used without purification unless otherwise noted. THF was freshly distilled from sodium/benzophenone ketyl prior to use. All other dry solvents were bought from Aldrich and used without further purification. N-iodomorpholine (NIM) was prepared according to the procedure of Hein *et al.*⁴⁰ Beloranib was prepared according to a described method.⁴⁹ The dimethyldioxirane (DMDO) solution was prepared and stored according to the procedure described by Adam *et al.*⁵⁰ The concentration of DMDO was determined via iodometric titration.

Enzyme Production for Biochemical Assays. C-terminal poly-His-tagged *EcMetAP* was obtained by expression in *E. coli* BL21(DE3) cells (Novagen) using an Arg-175-Gln mutant kindly provided by Prof. W.T. Lowther and Prof. B. Matthews. A detailed description of the preparation has been previously described.⁵¹ The gene for *HsMetAP1* was synthesized in an optimized nucleotide sequence for *E. coli* expression (Geneart) and cloned into the pET-28a(+) vector (Novagen) using *Bam*HI and *Sac*I cloning sites. The enzyme with a N-terminal His-tag was overexpressed in *E. coli* BL21(DE3) (Novagen) for 5 h at 37 °C. The enzyme was isolated and purified by nickel affinity chromatography (Chelating Sepharose Fast Flow, Amersham Biosciences; buffer: 50 mM Hepes pH 7.9, 500 mM KCl, 15 mM methionine, 10–250 mM imidazole gradient; removal of metal ions by adding EDTA pH 8.0 to a final concentration of 5 mM). The buffer was exchanged (storage buffer: 25 mM Hepes pH 7.9, 150 mM KCl, 15 mM methionine) and the enzyme stored at –80 °C. The *HsMetAP2* was produced in Sf9 cells using the Bac-to-Bac Baculovirus Expression System (Invitrogen). A detailed description of the cloning, expression, and isolation procedures has been previously described.⁴³

Biochemical Assays. Stock solutions for all assays were prepared in DMSO (10 mM) and stored at –20 °C. Assays were performed in 96 well plates (Greiner) at a total reaction volume of 100 μ L. First, enzyme (final concentration: 50 nM) was incubated with inhibitor (25 μ M) or positive control (DMSO, 0.25%) in a reaction buffer (final concentration: 100 μ M CoCl₂·6H₂O, 100 mM NaCl, 0.075% bovine serum albumine, 50 mM Tris pH 7.5) for 20 min at 37 °C. Then, the substrate Met-Gly-Met-Met was added to a final concentration of 400 μ M. After an incubation period of 15 min (*HsMetAP1*), 20 min (*EcMetAP*), or 60 min (*HsMetAP2*) at 37 °C, the enzyme reaction was stopped by adding 10 μ L 4% trifluoroacetic acid (TFA), and the plate was centrifuged at 1000g for 10 min. Detection of the product Gly-Met-Met was performed by HPLC: C18 column (Dr. Maisch, ReproSil-Pur 120 ODS-3, 3 μ m, 50 \times 2 mm). An 80 μ L injection volume was eluted with mobile phases A (H₂O and 0.1% TFA, filtered, degassed) and B (acetonitrile and 0.1% TFA, degassed) with the following profile: 10% \rightarrow 58% B linear gradient (4 min), 95% B (2 min), 10% B (2 min, re-equilibration). The product was quantified by UV absorption at 214 nm. Percentage inhibition was calculated as the ratio of Gly-Met-Met produced in the inhibited to uninhibited (positive control). IC₅₀ values were determined by measuring percent inhibition at a range of inhibitor concentrations and fitting to a logarithmic dose–response curve.

Cell Culture and Drug Treatment. Human umbilical vein endothelial cells (HUVECs; C-12203) were obtained from PromoCell GmbH and cultured in Endothelial Cell Growth Medium (C-22010; PromoCell GmbH). The fibrosarcoma cell line HT1080 was kindly provided by Dr. Marcus Renner (Institute of Pathology, University Hospital Heidelberg, Germany) and maintained in DMEM medium (Sigma-Aldrich) supplemented with 10% fetal bovine serum, 1% penicillin/streptomycin, 1 mM L-glutamine, and 0.5% Na-Pyruvate. Cells were cultured at 37 °C in a 5% CO₂ atmosphere. For viability assays, cells were seeded in 96-well plates (HUVECs: 2000 cells/well; HT1080: 2500 cells/well). For Western immunoblotting, HUVEC cells were seeded in six-well plates (150 000 cells/well). Treatment of cells with MetAP2 inhibitors was started 24 h after seeding to allow

cell attachment. Compounds (\pm)-31a, (\pm)-31b, (+)-31a, and (–)-31a were dissolved in DMSO as 10 mM stock solutions. Stock solutions were diluted 1:1000 in cell-type specific medium to prepare the treatment starting concentration (10 μ M; 0.1% DMSO). This starting concentration was diluted 1:2 in several diluting steps with cell-type specific medium to obtain 16 different concentrations ranging from 10 μ M to 0.3 nM. The seeding medium of the cells was aspirated and cells were incubated with 100 μ L/well (96-well plates) of the respective drug solution. As a control, cells were treated with 0.1% DMSO. Each drug concentration was performed in technical triplicates. The compound treatment was repeated every 24 h on three consecutive days until cell viability was measured. For Western immunoblotting, HUVECs were treated on three consecutive days with six different compound concentrations [(+)-31a and (–)-31a] prepared from the 10 mM stock solution (highest concentration: 5 μ M; 0.05% DMSO, lowest concentration: 1 nM). The seeding medium of the cells was aspirated, and cells were incubated with 1 mL/well (6-well plates) of the respective drug solution. As a control, cells were treated with 0.05% DMSO.

MTT Assay. Cell viability was analyzed 72 h after the first compound treatment using the MTT (3-[4,5-dimethylthiazol-2-yl]-2,5-diphenyltetrazolium bromide) assay according to the manufacturer's instructions (Sigma-Aldrich). In brief, cells were incubated with the MTT solution (0.5 mg mL^{–1} in medium) for 1 h at 37 °C. Afterward, the solution was removed and the tetrazolium salt was resolved in 100 μ L of DMSO/ethanol solution (1:2). Colorimetric measurement was performed at 570 nm using the FLUOstar Optima multidetection microplate reader (BMG Labtech). Data are presented as the mean \pm standard deviation. Dose–response curves were established by plotting growth (values normalized against DMSO control) against concentration (log) of compounds using the statistics software GraphPad Prism 6. The EC₅₀ was determined by computerized curve fitting using nonlinear regression.

Protein Sample Preparation and Western Immunoblotting. Cells were harvested 72 h after the first drug treatment. Total cell protein extracts were prepared by lysing cells in 20 μ L of cell lysis buffer (New England BioLabs) supplemented with Protease inhibitor mix (Serva Electrophoresis). Protein fractions were quantified (280 nm) and resuspended (80 μ g protein/sample) in Laemmli buffer for immunoblotting. Protein extracts were separated on a 15% sodium dodecyl sulfate polyacrylamide gel electrophoresis and electrotransferred to a nitrocellulose membrane. 14-3-3- γ (unprocessed form; 1:1500; Novus Biologicals, Littleton CO, USA), 14-3-3- γ (total; 1:500; Cell Signaling Technology), and actin (1:10000; MP Biomedicals) antibodies were diluted in TBST (Tris-buffered saline/Tween) supplemented with 5% milk powder and incubated at 4 °C overnight. The appropriate secondary antibody (LI-COR Biosciences) was applied [IRDye 800CW Donkey Anti-Mouse IgG (H+L) – 1:10 000 for anti-14-3-3- γ unprocessed form; IRDye 800CW Donkey Anti-Rabbit IgG (H+L) – 1:10 000 for anti-14-3-3- γ total; IRDye 680LT Donkey Anti-Mouse IgG (H+L) – 1:20 000 for antiactin] at RT for 1 h. Visualization was performed by enhanced infrared fluorescent with the Odyssey Sa Infrared Imaging System (LI-COR Biosciences).

Enzyme Production for Crystallization. A cDNA fragment corresponding to Gly108–Tyr478 was cloned into pFastBacHTa vector containing an N-terminal His-Tag followed by a TEV protease cleavage site. pFastBacHTa with the cloned *HsMetAP2* fragment was then used for transformation of DH10Bac *E. coli* cells to generate the recombinant bacmid, which was then used for the insect cells transfection and production of the recombinant baculovirus for the further protein expression. A cell pellet from 1 to 2 L of the insect cells was lysed in 40 mM Hepes (pH 7.4), 150 mM NaCl, 10% glycerol, 20 mM imidazole, +protease inhibitors, and DNase. The lysate was centrifuged at 48 000g for 45 min. The supernatant after filtering was applied to a HisTrap column equilibrated with 40 mM Hepes (pH 7.4), 150 mM NaCl, 10% glycerol, and 20 mM imidazole. The column was washed with several volumes of 40 mM Hepes (pH 7.4), 150 mM NaCl, 10% glycerol, and 20 mM imidazole, and additionally with 40 mM Hepes (pH 7.4), 1 M NaCl, 10% glycerol, and 20 mM imidazole.

The protein was eluted with a linear gradient from 20 to 500 mM imidazole in the same buffer. Fractions with MetAP2 were combined and dialyzed against 20 mM Hepes (pH 7.4), 150 mM NaCl, 5% glycerol O/N at 4 °C with TEV protease added to remove the HisTag (1:50 ratio). TEV protease, uncleaved MetAP2, and cleaved HisTag were removed by applying everything on the HisTrap column. The sample containing cleaved MetAP2 was concentrated to 5 mL and applied on a Superdex200 16/60 column equilibrated with 10 mM Hepes (pH 7.4), 150 mM NaCl and 10% glycerol. The selected fraction from the size exclusion step was then pooled and concentrated to 22 mg mL⁻¹. The protein sample was supplemented with CoCl₂ to a final concentration of 1 mM.

Enzyme Crystallization. The native crystals were obtained from similar conditions to those previously reported by Liu *et al.*: 50 mM sodium citrate buffer at pH 5.4 and 15% (v/v) *t*-butanol.¹⁹ Crystallization was performed using the hanging-drop vapor-diffusion method at 292 K in 24-well plates. The crystals appeared after a few days and were then used for soaking with (–)-31a, (+)-31a, (–)-31b, and (+)-31b: 0.5 μL of 50 mM inhibitor in 50% (v/v) DMSO, 50 mM sodium citrate buffer at pH 5.4, and 15% (v/v) *t*-butanol were added to the crystallization drop of 2–3 μL volume containing MetAP2 crystals.

Structure Determination and Refinement. Crystals were mounted in a nylon fiber loop and flash-cooled to 100 K in liquid nitrogen. The cryoprotection was performed for 2 s in reservoir solution complemented with 20% (v/v) glycerol. Diffraction data for MetAP2:(+)-31a and MetAP2:(–)-31a were collected on the ESRF ID23–2 beamline; those for MetAP2:(–)-31b were collected on the ID23–1 beamline and those for MetAP2:(+)-31b on the ESRF ID29 beamline. All data sets were indexed and integrated using XDS⁵² and scaled using SCALA.^{53,54} Intensities were converted to structure-factor amplitudes using the program TRUNCATE.⁵⁵ The structure of MetAP2 with all three compounds was solved by molecular replacement using the native MetAP2 structure published by Liu *et al.* (PDB: 1BNS).⁶ Model rebuilding was performed in COOT.⁵⁶ (+)-31a, (–)-31b, and (+)-31b were modeled manually. The refinement was done in REFMAC⁵⁷ using the maximum-likelihood target function. The stereochemical analysis of the final model was done in PROCHECK⁵⁸ and MolProbity.⁵⁹

■ ASSOCIATED CONTENT

■ Supporting Information

The Supporting Information is available free of charge on the ACS Publications website at DOI: 10.1021/acschembio.5b00755.

X-ray crystallographic data for 17a (CIF)

Synthetic chemistry procedures, compound characterization data, stability measurements, X-ray data, ¹H and ¹³C NMR spectra (PDF)

Accession Codes

The crystallographic data for 17a has been deposited with the Cambridge Crystallographic Data Centre as CCDC 894701. The atomic model and structure factors for the MetAP2: (+)-31a, MetAP2:(–)-31b, and MetAP2:(+)-31b complexes have been deposited with the Protein Data Bank as entries 5CLS, 5D6E, and 5D6F, respectively.

■ AUTHOR INFORMATION

Corresponding Author

*E-mail: aubry.miller@dkfz.de.

Author Contributions

[†]M. Morgen and C. Jöst contributed equally to this work.

Notes

The authors declare no competing financial interest.

■ ACKNOWLEDGMENTS

We thank N. De Vries, E. Ghebrai, J. Hummel-Eisenbeiss, B. Kraft, J. Lohbeck, H.-H. Schrenk, G. Schwebel, U. Wagner (DKFZ), S. Calcagno, A. Marschner, M. Wacker (IPMB), and V. Roman (HMGU) for technical assistance. We thank B. Hull and K. Klika for assistance with NMR spectroscopy and S. Barroso for suggesting the solvent-free Heck conditions. We thank the Hashmi group for IR spectra, the Helmchen group for use of their polarimeter, and Frank Rominger for the X-ray data for compound 17a (all from the Organic Chemistry Institute, Heidelberg University). We acknowledge the use of the X-ray crystallography platform of the Helmholtz Zentrum München. This work was supported by the DKFZ Intramural Fund (A.K.M. and C.D.K.), the DKFZ Development Fund (A.K.M. and N.G.), and Deutsche Krebshilfe (C.D.K.). Financial support from the Helmholtz Drug Initiative and the German Consortium for Translational Research (DKTK) is gratefully acknowledged. Protein X-ray graphics and analyses were performed with the UCSF Chimera package. Chimera is developed by the Resource for Biocomputing, Visualization, and Informatics at the University of California, San Francisco (supported by NIGMS P41-GM103311).

■ REFERENCES

- (1) Li, J. W. H., and Vederas, J. C. (2009) Drug discovery and natural products: end of an era or an endless frontier? *Science* 325, 161–165.
- (2) Ingber, D., Fujita, T., Kishimoto, S., Sudo, K., Kanamaru, T., Brem, H., and Folkman, J. (1990) Synthetic analogues of fumagillin that inhibit angiogenesis and suppress tumour growth. *Nature* 348, 555–557.
- (3) Marui, S., Itoh, F., Kozai, Y., Sudo, K., and Kishimoto, S. (1992) Chemical modification of fumagillin. I. 6-O-acyl, 6-O-sulfonyl, 6-O-alkyl, and 6-O-(N-substituted-carbamoyl)fumagillols. *Chem. Pharm. Bull.* 40, 96–101.
- (4) Marui, S., and Kishimoto, S. (1992) Chemical modification of fumagillin. II. 6-Amino-6-deoxyfumagillol and its derivatives. *Chem. Pharm. Bull.* 40, 575–579.
- (5) Marui, S., Yamamoto, T., Sudo, K., Akimoto, H., and Kishimoto, S. (1995) Chemical modification of fumagillin. III. Modification of the spiro-epoxide. *Chem. Pharm. Bull.* 43, 588–593.
- (6) Turk, B. E., Su, Z., and Liu, J. O. (1998) Synthetic analogues of TNP-470 and ovalicin reveal a common molecular basis for inhibition of angiogenesis and immunosuppression. *Bioorg. Med. Chem.* 6, 1163–1169.
- (7) Han, C. K., Ahn, S. K., Choi, N. S., Hong, R. K., Moon, S. K., Chun, H. S., Lee, S. J., Kim, J. W., Hong, C. I., Kim, D., Yoon, J. H., and No, K. T. (2000) Design and synthesis of highly potent fumagillin analogues from homology modeling for a human MetAP-2. *Bioorg. Med. Chem. Lett.* 10, 39–43.
- (8) Fardis, M., Pyun, H.-J., Tario, J., Jin, H., Kim, C. U., Ruckman, J., Lin, Y., Green, L., and Hicke, B. (2003) Design, synthesis and evaluation of a series of novel fumagillin analogues. *Bioorg. Med. Chem.* 11, 5051–5058.
- (9) Zhou, G., Tsai, C. W., and Liu, J. O. (2003) Fumagalone, a Reversible Inhibitor of Type 2 Methionine Aminopeptidase and Angiogenesis. *J. Med. Chem.* 46, 3452–3454.
- (10) Pyun, H.-J., Fardis, M., Tario, J., Yang, C. Y., Ruckman, J., Henninger, D., Jin, H., and Kim, C. U. (2004) Investigation of novel fumagillin analogues as angiogenesis inhibitors. *Bioorg. Med. Chem. Lett.* 14, 91–94.
- (11) Lu, J., Chong, C. R., Hu, X., and Liu, J. O. (2006) Fumarranol, a Rearranged Fumagillin Analogue That Inhibits Angiogenesis in Vivo. *J. Med. Chem.* 49, 5645–5648.
- (12) Lee, H. W., Cho, C. S., Kang, S. K., Yoo, Y. S., Shin, J. S., and Ahn, S. K. (2007) Design, Synthesis, and Antiangiogenic Effects of a

Series of Potent Novel Fumagillin Analogues. *Chem. Pharm. Bull.* 55, 1024–1029.

(13) Arico-Muendel, C. C., Benjamin, D. R., Caiazzo, T. M., Centrella, P. A., Contonio, B. D., Cook, C. M., Doyle, E. G., Hannig, G., Labenski, M. T., Searle, L. L., Lind, K., Morgan, B. A., Olson, G., Paradise, C. L., Self, C., Skinner, S. R., Sluboski, B., Svendsen, J. L., Thompson, C. D., Westlin, W., and White, K. F. (2009) Carbamate Analogues of Fumagillin as Potent, Targeted Inhibitors of Methionine Aminopeptidase-2. *J. Med. Chem.* 52, 8047–8056.

(14) Yin, S. Q., Wang, J. J., Zhang, C. M., and Liu, Z. P. (2012) The development of MetAP-2 inhibitors in cancer treatment. *Curr. Med. Chem.* 19, 1021–1035.

(15) Joharapurkar, A. A., Dhanesha, N. A., and Jain, M. R. (2014) Inhibition of the methionine aminopeptidase 2 enzyme for the treatment of obesity. *Diabetes, Metab. Syndr. Obes.: Targets Ther.* 7, 73–84.

(16) Griffith, E. C., Su, Z., Niwayama, S., Ramsay, C. A., Chang, Y.-H., and Liu, J. O. (1998) Molecular recognition of angiogenesis inhibitors fumagillin and ovalicin by methionine aminopeptidase 2. *Proc. Natl. Acad. Sci. U. S. A.* 95, 15183–15188.

(17) Griffith, E. C., Su, Z., Turk, B. E., Chen, S., Chang, Y.-H., Wu, Z., Biemann, K., and Liu, J. O. (1997) Methionine aminopeptidase (type 2) is the common target for angiogenesis inhibitors AGM-1470 and ovalicin. *Chem. Biol.* 4, 461–471.

(18) Sin, N., Meng, L., Wang, M. Q. W., Wen, J. J., Bornmann, W. G., and Crews, C. M. (1997) The anti-angiogenic agent fumagillin covalently binds and inhibits the methionine aminopeptidase, MetAP-2. *Proc. Natl. Acad. Sci. U. S. A.* 94, 6099–6103.

(19) Liu, S., Widom, J., Kemp, C. W., Crews, C. M., and Clardy, J. (1998) Structure of Human Methionine Aminopeptidase-2 Complexed with Fumagillin. *Science* 282, 1324–1327.

(20) Yeh, J.-R. J., Mohan, R., and Crews, C. M. (2000) The antiangiogenic agent TNP-470 requires p53 and p21CIP/WAF for endothelial cell growth arrest. *Proc. Natl. Acad. Sci. U. S. A.* 97, 12782–12787.

(21) Zhang, Y., Griffith, E. C., Sage, J., Jacks, T., and Liu, J. O. (2000) Cell cycle inhibition by the anti-angiogenic agent TNP-470 is mediated by p53 and p21WAF1/CIP1. *Proc. Natl. Acad. Sci. U. S. A.* 97, 6427–6432.

(22) Hines, J., Ju, R., Dutschman, G. E., Cheng, Y.-C., and Crews, C. M. (2010) Reversal of TNP-470-induced endothelial cell growth arrest by guanine and guanine nucleosides. *J. Pharmacol. Exp. Ther.* 334, 729–738.

(23) Sundberg, T. B., Darricarrere, N., Cirone, P., Li, X., McDonald, L., Mei, X., Westlake, C. J., Slusarski, D. C., Beynon, R. J., and Crews, C. M. (2011) Disruption of Wnt planar cell polarity signaling by aberrant accumulation of the MetAP-2 substrate Rab37. *Chem. Biol.* 18, 1300–1311.

(24) Datta, B., Majumdar, A., Datta, R., and Balusu, R. (2004) Treatment of Cells with the Angiogenic Inhibitor Fumagillin Results in Increased Stability of Eukaryotic Initiation Factor 2-Associated Glycoprotein, p67, and Reduced Phosphorylation of Extracellular Signal-Regulated Kinases. *Biochemistry* 43, 14821–14831.

(25) Bhargava, P., Marshall, J. L., Rizvi, N., Dahut, W., Yoe, J., Figueroa, M., Phipps, K., Ong, V. S., Kato, A., and Hawkins, M. J. (1999) A Phase I and pharmacokinetic study of TNP-470 administered weekly to patients with advanced cancer. *Clin. Cancer Res.* 5, 1989–1995.

(26) Stadler, W. M., Kuzel, T., Shapiro, C., Sosman, J., Clark, J., and Vogelzang, N. J. (1999) Multi-Institutional Study of the Angiogenesis Inhibitor TNP-470 in Metastatic Renal Carcinoma. *J. Clin. Oncol.* 17, 2541–2545.

(27) Shin, S. J., Jeung, H.-C., Ahn, J. B., Rha, S. Y., Roh, J. K., Park, K. S., Kim, D.-H., Kim, C., and Chung, H. C. (2010) A phase I pharmacokinetic and pharmacodynamic study of CKD-732, an antiangiogenic agent, in patients with refractory solid cancer. *Invest. New Drugs* 28, 650–658.

(28) Arico-Muendel, C. C., Belanger, B., Benjamin, D., Blanchette, H. S., Caiazzo, T. M., Centrella, P. A., DeLorey, J., Doyle, E. G.,

Gradhand, U., Griffin, S. T., Hill, S., Labenski, M. T., Morgan, B. A., O'Donovan, G., Prasad, K., Skinner, S., Taghizadeh, N., Thompson, C. D., Wakefield, J., Westlin, W., and White, K. F. (2013) Metabolites of PPI-2458, a selective, irreversible inhibitor of methionine aminopeptidase-2: structure determination and in vivo activity. *Drug Metab. Dispos.* 41, 814–826.

(29) Arico-Muendel, C. C., Blanchette, H., Benjamin, D. R., Caiazzo, T. M., Centrella, P. A., DeLorey, J., Doyle, E. G., Johnson, S. R., Labenski, M. T., Morgan, B. A., O'Donovan, G., Sarjeant, A. A., Skinner, S., Thompson, C. D., Griffin, S. T., Westlin, W., and White, K. F. (2013) Orally Active Fumagillin Analogues: Transformations of a Reactive Warhead in the Gastric Environment. *ACS Med. Chem. Lett.* 4, 381–386.

(30) Baldwin, J. E., Bulger, P. G., and Marquez, R. (2002) Fast and efficient synthesis of novel fumagillin analogues. *Tetrahedron* 58, 5441–5452.

(31) Jeong, B.-S., Choi, N. S., Ahn, S. K., Bae, H., Kim, H. S., and Kim, D. (2005) Total synthesis and antiangiogenic activity of cyclopentane analogues of fumagillol. *Bioorg. Med. Chem. Lett.* 15, 3580–3583.

(32) Mazitschek, R., Huwe, A., and Giannis, A. (2005) Synthesis and biological evaluation of novel fumagillin and ovalicin analogues. *Org. Biomol. Chem.* 3, 2150–2154.

(33) Rodeschini, V., Boiteau, J.-G., Van de Weghe, P., Tarnus, C., and Eustache, J. (2004) MetAP-2 Inhibitors Based on the Fumagillin Structure. Side-Chain Modification and Ring-Substituted Analogues. *J. Org. Chem.* 69, 357–373.

(34) Rodeschini, V., de Weghe, P. V., Tarnus, C., and Eustache, J. (2005) A simple spiroepoxide as methionine aminopeptidase-2 inhibitor: synthetic problems and solutions. *Tetrahedron Lett.* 46, 6691–6695.

(35) Rodeschini, V., Van de Weghe, P., Salomon, E., Tarnus, C., and Eustache, J. (2005) Enantioselective Approaches to Potential MetAP-2 Reversible Inhibitors. *J. Org. Chem.* 70, 2409–2412.

(36) Miller, A.; Jöst, C.; Klein C. New spiroepoxide tetrahydrobenzotriazoles useful as MetAP-II inhibitors. PCT Pat. Appl. WO2014044399 A1, 2014.

(37) Goncalves-Martin, M. G., Saxer, A., and Renaud, P. (2009) A practical synthesis of (S)-cyclopent-2-enol. *Synlett* 2009, 2801–2802.

(38) Li, J., Yan, W., and Kishi, Y. (2015) Unified Synthesis of C1–C19 Building Blocks of Halichondrins via Selective Activation/Coupling of Polyhalogenated Nucleophiles in (Ni)/Cr-Mediated Reactions. *J. Am. Chem. Soc.* 137, 6226–6231.

(39) Witulski, B., and Alayrac, C. (2006) Product subclass 1:1-haloalk-1-ynes and alk-1-yn-1-ols. *Sci. Synth.* 24, 905–932.

(40) Hein, J. E., Tripp, J. C., Krasnova, L. B., Sharpless, K. B., and Fokin, V. V. (2009) Copper(I)-catalyzed cycloaddition of organic azides and 1-iodoalkynes. *Angew. Chem., Int. Ed.* 48, 8018–8021.

(41) Schulman, J. M., Friedman, A. A., Pantelev, J., and Lautens, M. (2012) Synthesis of 1,2,3-triazole-fused heterocycles via Pd-catalyzed cyclization of 5-iodotriazoles. *Chem. Commun.* 48, 55–57.

(42) Jeffery, T. (1996) On the efficiency of tetraalkylammonium salts in Heck type reactions. *Tetrahedron* 52, 10113–10130.

(43) Altmeyer, M. A., Marschner, A., Schiffmann, R., and Klein, C. D. (2010) Subtype-selectivity of metal-dependent methionine aminopeptidase inhibitors. *Bioorg. Med. Chem. Lett.* 20, 4038–4044.

(44) Calo, V., Nacci, A., Monopoli, A., and Cotugno, P. (2009) Heck reactions with palladium nanoparticles in ionic liquids: coupling of aryl chlorides with deactivated olefins. *Angew. Chem., Int. Ed.* 48, 6101–6103.

(45) Copeland, R. A. (2013) *Evaluation of enzyme inhibitors in drug discovery: a guide for medicinal chemists and pharmacologists*, 2nd ed., Wiley, Hoboken, NJ.

(46) Tucker, L. A., Zhang, Q., Sheppard, G. S., Lou, P., Jiang, F., McKeegan, E., Lesniewski, R., Davidsen, S. K., Bell, R. L., and Wang, J. (2008) Ectopic expression of methionine aminopeptidase-2 causes cell transformation and stimulates proliferation. *Oncogene* 27, 3967–3976.

(47) Kusaka, M., Sudo, K., Matsutani, E., Kozani, Y., Marui, S., Fujita, T., Inger, D., and Folkman, J. (1994) Cytostatic inhibition of

endothelial cell growth by the angiogenesis inhibitor TNP-470 (AGM-1470). *Br. J. Cancer* 69, 212–216.

(48) Towbin, H., Bair, K. W., DeCaprio, J. A., Eck, M. J., Kim, S., Kinder, F. R., Morollo, A., Mueller, D. R., Schindler, P., Song, H. K., van, O. J., Versace, R. W., Voshol, H., Wood, J., Zabudoff, S., and Phillips, P. E. (2003) Proteomics-based Target Identification: Bengamides as a new class of methionine aminopeptidase inhibitors. *J. Biol. Chem.* 278, 52964–52971.

(49) Crawford, T., Reece H. A. (2012) Crystalline Solids of a MetAP-2 Inhibitor and Methods of Making and Using Same. PCT Pat. Appl. WO2012064838 A1.

(50) Adam, W., Bialas, J., and Hadjarapoglou, L. (1991) A Convenient Preparation of Acetone Solutions of Dimethyldioxirane. *Chem. Ber.* 124, 2377.

(51) Lowther, W. T., McMillen, D. A., Orville, A. M., and Matthews, B. W. (1998) The anti-angiogenic agent fumagillin covalently modifies a conserved active-site histidine in the Escherichia coli methionine aminopeptidase. *Proc. Natl. Acad. Sci. U. S. A.* 95, 12153–12157.

(52) Kabsch, W. (2010) XDS. *Acta Crystallogr., Sect. D: Biol. Crystallogr.* 66, 125–132.

(53) Evans, P. (2006) Scaling and assessment of data quality. *Acta Crystallogr., Sect. D: Biol. Crystallogr.* 62, 72–82.

(54) Winn, M. D., Ballard, C. C., Cowtan, K. D., Dodson, E. J., Emsley, P., Evans, P. R., Keegan, R. M., Krissinel, E. B., Leslie, A. G., McCoy, A., McNicholas, S. J., Murshudov, G. N., Pannu, N. S., Potterton, E. A., Powell, H. R., Read, R. J., Vagin, A., and Wilson, K. S. (2011) Overview of the CCP4 suite and current developments. *Acta Crystallogr., Sect. D: Biol. Crystallogr.* 67, 235–242.

(55) French, S., and Wilson, K. (1978) On the treatment of negative intensity observations. *Acta Crystallogr., Sect. A: Cryst. Phys., Diffraction, Theor. Gen. Crystallogr.* 34, 517–525.

(56) Emsley, P., Lohkamp, B., Scott, W. G., and Cowtan, K. (2010) Features and development of Coot. *Acta Crystallogr., Sect. D: Biol. Crystallogr.* 66, 486–501.

(57) Murshudov, G. N., Vagin, A. A., and Dodson, E. J. (1997) Refinement of macromolecular structures by the maximum-likelihood method. *Acta Crystallogr., Sect. D: Biol. Crystallogr.* 53, 240–255.

(58) Laskowski, R. A., MacArthur, M. W., Moss, D. S., and Thornton, J. M. (1993) PROCHECK: a program to check the stereochemical quality of protein structures. *J. Appl. Crystallogr.* 26, 283–291.

(59) Chen, V. B., Arendall, W. B., 3rd, Headd, J. J., Keedy, D. A., Immormino, R. M., Kapral, G. J., Murray, L. W., Richardson, J. S., and Richardson, D. C. (2010) MolProbity: all-atom structure validation for macromolecular crystallography. *Acta Crystallogr., Sect. D: Biol. Crystallogr.* 66, 12–21.